ELSEVIER

Journal of Power Sources 113 (2003) 1–10

JOURNAL OF POWER SOURCES

www.elsevier.com/locate/jpowsour

Development of lanthanum ferrite SOFC cathodes

S.P. Simner*, J.F. Bonnett, N.L. Canfield, K.D. Meinhardt, J.P. Shelton, V.L. Sprenkle, J.W. Stevenson

Materials Sciences Department, Pacific Northwest National Laboratory, 902 Battelle Boulevard, P.O. Box 999, Richland, WA 99352, USA

Received 9 August 2002; accepted 18 August 2002

Abstract

A number of studies have been conducted concerning compositional/microstructural modifications of a Sr-doped lanthanum ferrite (LSF) cathode and protective Sm-doped ceria (SDC) layer in an anode supported solid oxide fuel cell (SOFC). Emphasis was placed on achieving enhanced low temperature (700–800 °C) performance, and long-term cell stability. Investigations involved manipulation of the lanthanum ferrite chemistry, addition of noble metal oxygen reduction catalysts, incorporation of active cathode layer compositions containing Co, Fe and higher Sr contents, and attempts to optimize the ceria barrier layer between the LSF cathode and YSZ electrolyte.

Keywords: SOFC; Lanthanum ferrite; SDC

1. Introduction

The purpose of this paper is to detail recent investigations at Pacific Northwest National Laboratory (PNNL) directed towards the improved lower temperature (700–800 °C) performance of anode-supported solid oxide fuel cells (SOFCs) by optimizing the cathode and its interfaces. It is widely established that the performance of low-temperature SOFCs is highly dependent on cathode polarization losses, which must be minimized to optimize the SOFC power densities. In our own research $La_{0.8}Sr_{0.2}FeO_{3-\delta}$ (LSF-20) has demonstrated high power outputs (~0.9–0.95 W/cm^2 at 750 °C/0.7 V), and good long-term stability [1]. It should be noted that the aforementioned performance is atypical, and a more consistent, reproducible power value is 0.75–0.8 W/cm^2 (750 °C/0.7 V). The exact phenomena behind the inconsistencies have not been precisely established, though this subject and possible explanations will be considered throughout the text. Other perovskite compositions previously considered at PNNL with Co, Ni and Mn B-site cations have indicated either poor chemical, and long-term performance stability, or the materials simply exhibited lower power densities than our optimized LSF cathode. Therefore, most of the recent cathode research efforts at PNNL have been directed towards LSF. This present study predominantly considers non-stoichiometric LSF-20 compositions, $(La_{0.8}Sr_{0.2})_xFeO_{3-\delta}$ ($x = 0.95$–1.05), the addition of second phases to the LSF (in particular ceria and noble metals), and optimization of the relevant microstructures and interfaces in an attempt to enhance the ultimate cell performance and longevity.

2. Experimental

Anode (NiO–YSZ)–electrolyte (YSZ) substrate samples were produced via standard organic tape casting and tape lamination procedures, co-sintered at 1375 °C for 1 h, and subsequently creep-flattened at 1350 °C for 2 h. The post-sintered/post-reduced anode (~500 μm thick) was comprised of a bulk layer with a solids ratio of 40/60 vol.% Ni/YSZ (and approximately 30 vol.% porosity), and a 5–10 μm thick active anode layer with 50/50 vol.% solids Ni/YSZ. The sintered thickness of the YSZ membrane was 5–10 μm thick. All cathode and $Ce_{0.8}Sm_{0.2}O_{1.9}$ (SDC-20) powders used in this investigation were synthesized using a glycine-nitrate combustion technique [2]. Post-synthesized powders were typically calcined from 1000 to 1200 °C for 1 h, and then attrition milled for 10–30 min to achieve the desired particle size distribution (typically $d_{50} < 1$ μm, $d_{90} < 2$ μm). SDC-20 interlayers (~5 μm post-sintered thickness) were applied to creep-flattened anode substrates via screen-printing, and sintered from 1100 to 1300 °C for 2 h.

* Corresponding author. Tel.: +1-509-943-6264; fax: +1-509-375-2186.
E-mail address: steven.simner@pnl.gov (S.P. Simner).

0378-7753/02/$ – see front matter
PII: S0378-7753(02)00455-X

The cathodes were also applied by screen-printing (25–40 μm post-sintered thickness). Cathode compositions were typically sintered from 1100 to 1250 °C. The diameter of the anode support was 25 mm, and that of the screen-printed cathode initially 22 mm. Recently, however, concerns of chemical interaction between the cathode and the seal material have led to a decrease in the cathode diameter to 19.5 mm. The cathode area was used as the active cell area to calculate current and power densities. Screen-printed Pt grids with embedded Pt gauze, and screen-printed NiO grids with embedded Ni gauze were used as current collectors for the cathode and anode, respectively. Figs. 1 and 2 show a schematic of the single cell set-up, and a photo of the cell (air side) in place on the test fixture, respectively. The cells were sealed to alumina test fixtures using Aremco cements, and current–voltage data recorded from 700 to 850 °C using an Arbin BT2000 potentiostat–galvanostat electrochemical testing system. Cells were held at 0.7 V and periodically subjected to current sweeps from 0 to 7 A. A 97% H_2–3% H_2O gas mixture was flowed to the anode at 200 sccm, and air to the cathode at 300 sccm. At least two samples of each cathode composition were analyzed to verify cell performances. Thermal expansion in air was conducted on sintered bars (∼25 mm × 3 mm × 3 mm) using a Unitherm model 1161 dilatometer.

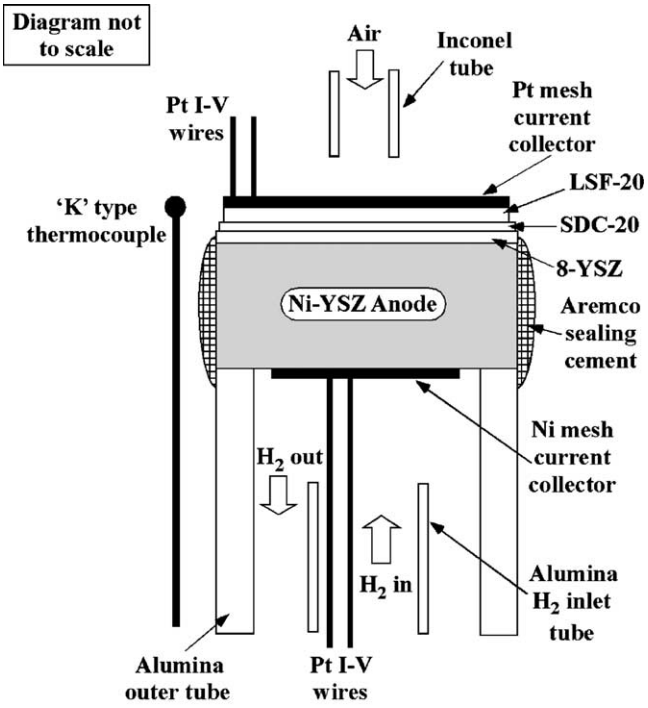

Fig. 1. Schematic of single cell apparatus.

3. Results and discussion

It is important to note that the studies reported in this paper have been conducted over an 12–18-month period, during which time the performance of the base LSF material has periodically changed to a small degree, apparently coinciding with the use of newly synthesized powder batches. Laboratory scale processing typically enables the production of a 200 g batch of powder, and approximately every 3 months a new batch is required. Despite maintaining established protocols for powder synthesis each powder batch indicates a slight degree of performance variation. As such it is not possible to directly compare each and every result to be presented in this paper. However, within each given investigation all powders used were taken from the same synthesis batch, and hence at the very least these

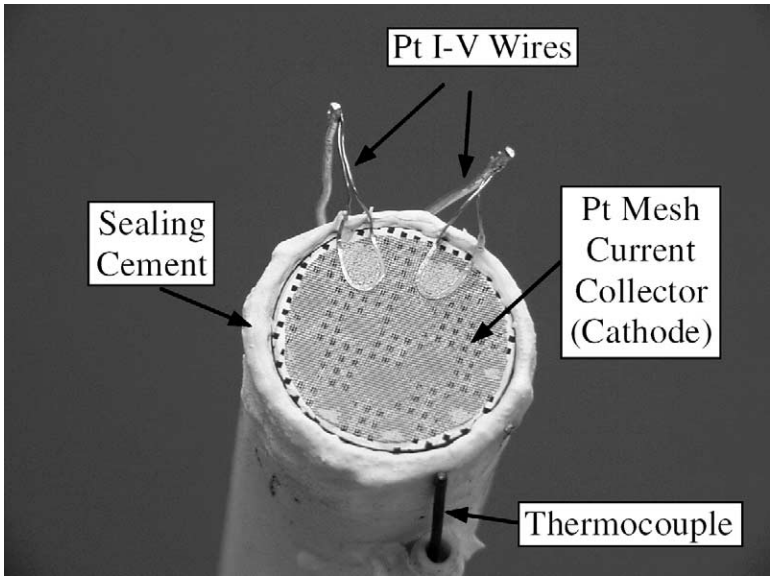

Fig. 2. Photograph of single cell apparatus—cathode side.

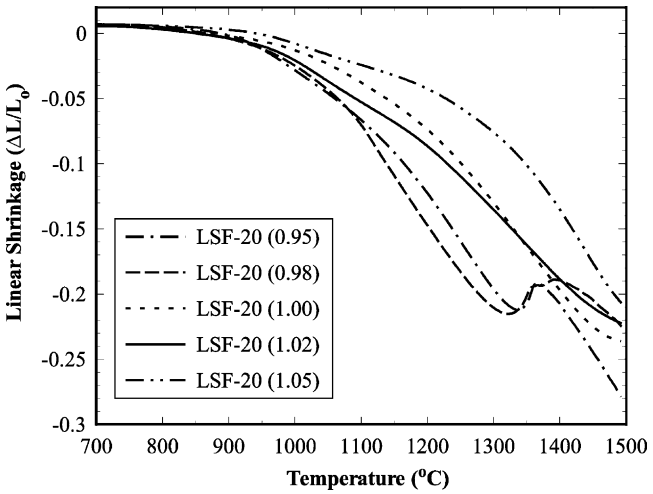

Fig. 3. Sintering shrinkage behavior of $(La_{0.8}Sr_{0.2})_xFeO_{3-\delta}$ ($x = 0.95$–1.05).

results can be confidently compared and hopefully accurate conclusions drawn.

3.1. Non-stoichiometric $(La_{0.8}Sr_{0.2})_xFeO_{3-\delta}$ compositions

Many perovskites, in particular lanthanum chromites [3–5], exhibit markedly different sintering characteristics with small variations in A/B stoichiometry. Varied sintering characteristics can in turn lead to over- or under-sintering of the cathode (at a given temperature), and subsequent performance reduction due to lack of porosity or insufficient cathode adherence. Slight variations in the A/B ratio are, however, not expected to significantly affect physical characteristics such as electrical conductivity and thermal expansion. Compositions of the form $(La_{0.8}Sr_{0.2})_xFeO_{3-\delta}$, where $x = 0.95$, 0.98, 1.00, 1.02 and 1.05, were considered. Fig. 3 shows the sintering shrinkage behavior of the investigated compositions (calcined at 800 °C/4 h). To provide an idea of the varied sintering behaviors of these compositions, for $x = 0.98$ a 15% shrinkage is achieved by ~1150 °C compared to 1350 °C for $x = 1.05$. A-site depleted samples exhibit enhanced densification while B-site depleted compositions show retarded sintering behavior compared to the stoichiometric A/B = 1 composition. Fig. 4 shows XRD traces for each composition after calcination at 1200 °C. Compositions with $x = 1.00$ appeared relatively phase pure (possibly containing a trace phase tentatively identified as $Sr_7Fe_{10}O_{22}$), while samples with $x > 1.00$ indicated SrLaFeO$_4$ as an additional phase. Interestingly A/B < 1.00 compositions do not show a precipitated Fe-O phase, and A/B > 1.00 no La-O phases. La_2O_3 is often observed in B-site depleted manganites and chromites, and extremely detrimental to sample integrity due to hydration, and subsequent volume expansion, of the oxide. Fig. 5(a) and (b) indicate *I–V* data at 700 °C for the aforementioned compositions (sintered at 1150 °C/2 h) at 0 h (start of test) and 72 h. For diagram clarity the power curves have been omitted but power densities can be easily established knowing the active cathode area is 3 cm^2. Not surprisingly, the $x = 1.00$

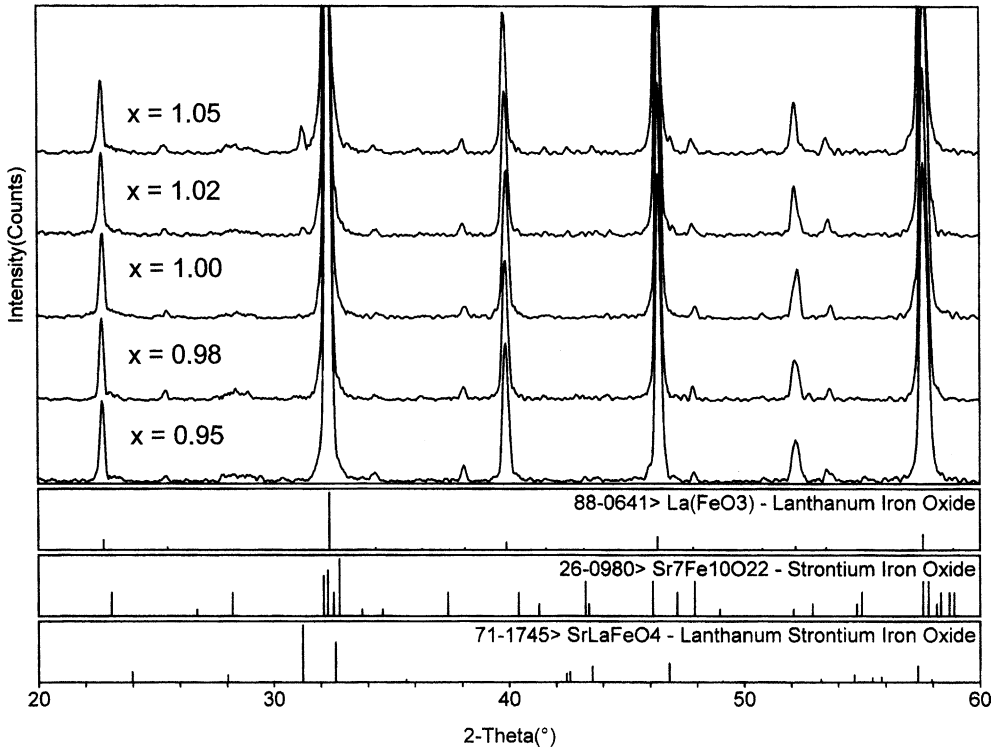

Fig. 4. X-ray diffraction data for $(La_{0.8}Sr_{0.2})_xFeO_{3-\delta}$ ($x = 0.95$–1.05) after calcination at 1200 °C.

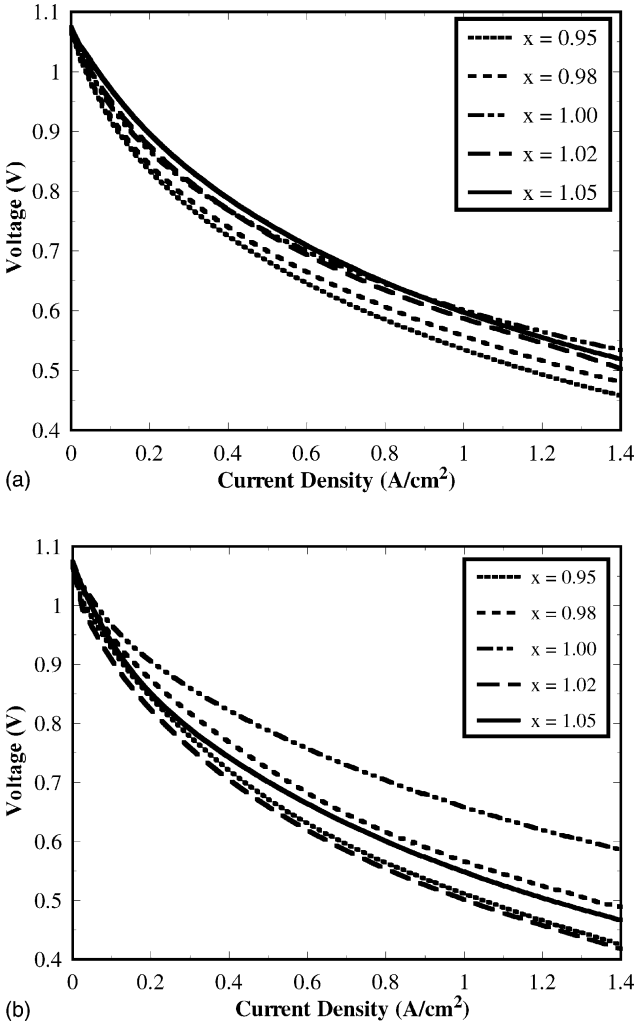

Fig. 5. Current–voltage data for $(La_{0.8}Sr_{0.2})_xFeO_{3-\delta}$ ($x = 0.95$–1.05) at 700 °C after (a) 0 h, and (b) 72 h.

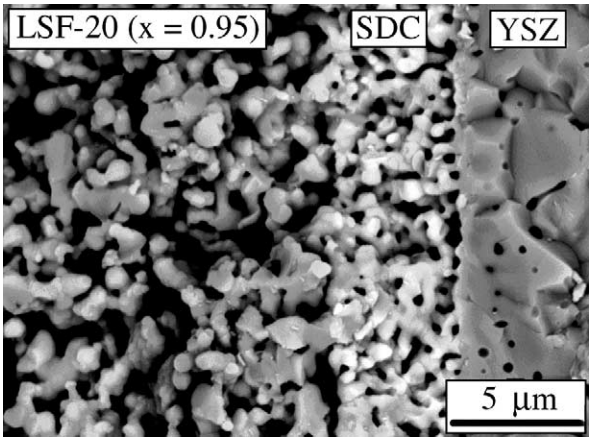

Fig. 6. SEM micrograph of an anode-supported YSZ cell utilizing a $(La_{0.8}Sr_{0.2})_{0.95}FeO_{3-\delta}$ cathode sintered at 1150 °C for 2 h.

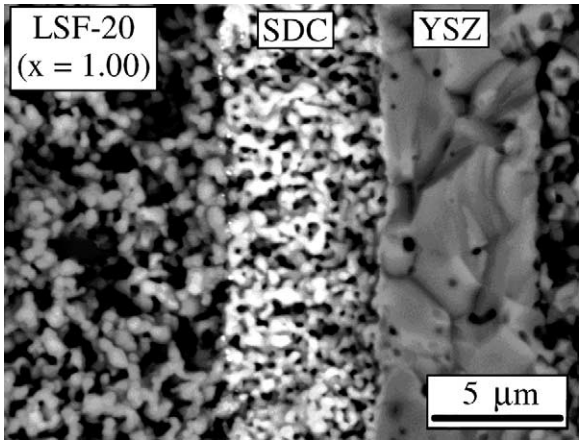

Fig. 7. SEM micrograph of an anode-supported YSZ cell utilizing a $La_{0.8}Sr_{0.2}FeO_{3-\delta}$ cathode sintered at 1150 °C for 2 h.

composition indicates the best cell performance for cathodes sintered at 1150 °C. This sintering temperature had previously been established as the optimum sintering temperature for LSF-20 ($x = 1.00$) [1], and hence the non-stoichiometric compositions are likely either over-sintered (for $x < 1.00$) or poorly adhered (for $x > 1.00$). Indeed SEM of the LSF-20 ($x = 0.95$) sample (Fig. 6) indicates coarser particles in both LSF and Sm-doped ceria (SDC) layers compared to LSF-20 ($x = 1.00$) (Fig. 7). Larger particles in the LSF-20 ($x = 0.95$) are simply due to over-sintering (coarsening) of the microstructure. The disparity between the morphology of the SDC layer for $x = 0.95$ and 1.00 is explained by the presence of high proportions of Fe in the SDC interlayer (detected by EDX). As will be described in greater detail later in this paper the incorporation of transition metal cations into the SDC layer can have a marked affect on the sintering and microstructural evolution of this layer. It may be possible to sinter the LSF-20 ($x < 1.00$) compositions at lower temperatures to prevent particle coarsening and Fe diffusion into the SDC layer, but with

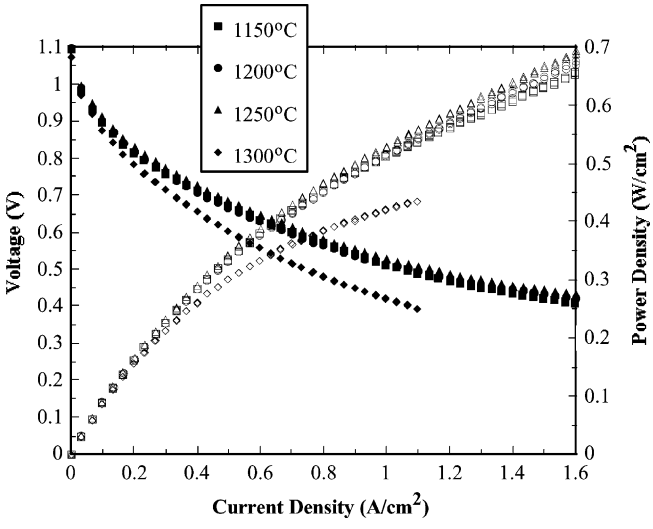

Fig. 8. Current–voltage data at 700 °C for an anode-supported YSZ cell utilizing a $La_{0.8}Sr_{0.2}FeO_{3-\delta}$ cathode (1150 °C/2h) and $Ce_{0.8}Sm_{0.2}O_{1.9}$ interlayer (1150–1300 °C/2 h).

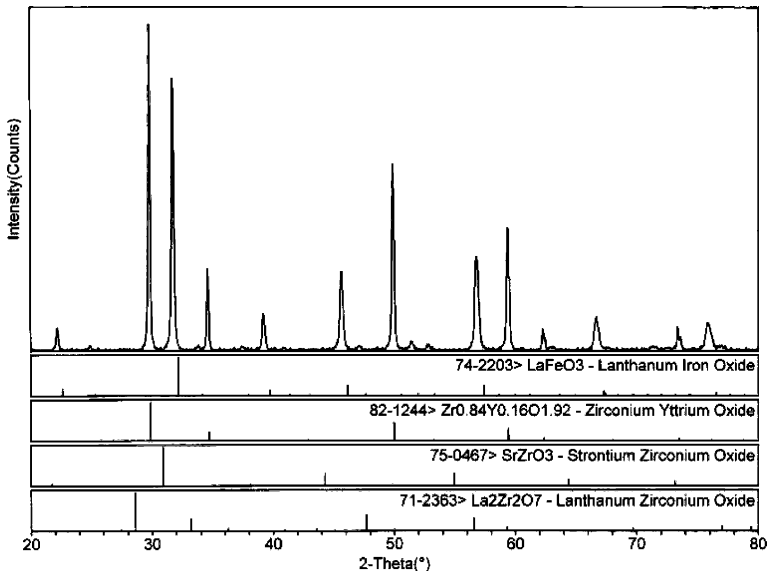

Fig. 9. X-ray diffraction data indicating no Sr-La zirconate formation after reaction of 8-YSZ and LSF-20 at 1200 °C for 2 h.

respect to the LSF-20 ($x > 1.00$) samples, which appear to be under-sintered, using higher temperatures is probably not possible for two reasons. Firstly, above 1200 °C YSZ reacts with doped ceria to form a resistive interfacial layer [6]—Fig. 8 illustrates reduced performance for cells with SDC interlayers applied above 1250 °C. Secondly, preliminary studies on LSF cathode-supported cells at PNNL have shown that above ~1250 °C La readily diffuses from the cathode into the SDC layer—studies by Eguchi et al. [7] indicate that La incorporation reduces the ionic conductivity of doped ceria materials. What this does indicate is that slight variations in stoichiometry can dramatically affect the cell performance, and that highly accurate standardization of precursor solutions is required to ensure optimal and reproducible data. As expected, the thermal expansion of LSF-20 showed little dependence on the A/B ratio, and was measured to be between 12.50×10^{-6} and 12.65×10^{-6} °C^{-1} for LSF-20 ($x = 0.95$–1.05) (25–1200 °C).

3.2. SDC with transition metal dopants

The exact role of the Sm-doped ceria layer has not been established though previous data at PNNL has indicated significant performance improvements when the ceria layer is present between the LSF cathode and the YSZ electrolyte [8]. Reaction of iso-statically pressed LSF-20 and YSZ powder mixtures at 1200 °C (Fig. 9) indicates no La- or Sr-zirconate formation (this is in agreement with Ralph et al. [9])—zirconate formation is typically observed with cobaltite and manganite cathodes on a YSZ electrolyte [10–14]. However, a small shift in the LSF peak positions indicating increased unit cell volume (240–247 Å^3) is apparent. Even after reaction at 1400 °C for 24 h no zirconate phases could be positively identified, though trace phases (with peak intensities barely above background) indicated possible matches with $SrFe_{12}O_{19}$, ZrO_2, $SrZrO_3$, SrY_2O_4 and $Sr_3Zr_2O_7$. This aforementioned peak shift (LSF–YSZ reacted at 1200 °C) phenomenon and its implications are under investigation, and will be reported in a future article. Currently, it is assumed that the improved cell performance observed when a ceria layer is present is a consequence of the higher ionic conductivity and surface exchange kinetics of SDC relative to YSZ.

Though the precise function of the SDC layer is not understood, it is generally accepted that since this layer is an ionic conductor (and hence an extension of the electrolyte), it should be of sufficiently high density to maximize ionic transport through the layer, and cathode reaction sites at the LSF–SDC interface. However, the SDC layer is applied onto a post-sintered anode–YSZ substrate (rather than co-fired with the anode support) to avoid detrimental SDC–YSZ interactions at the anode-support firing temperature close to 1400 °C. As such, sintering of the SDC is

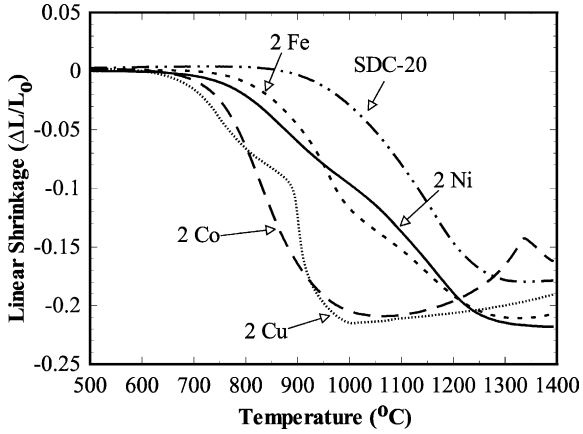

Fig. 10. Sintering shrinkage data for $Ce_{0.8}Sm_{0.18}M_{0.02}O_{1.9}$ compositions where M = Co, Cu, Fe and Ni.

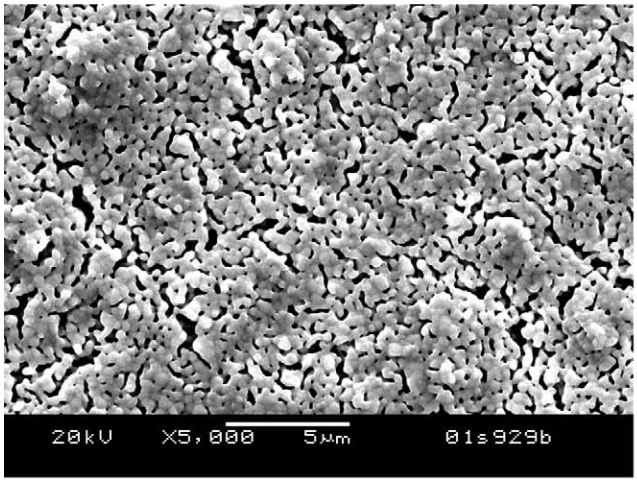

(a) – SDC-20

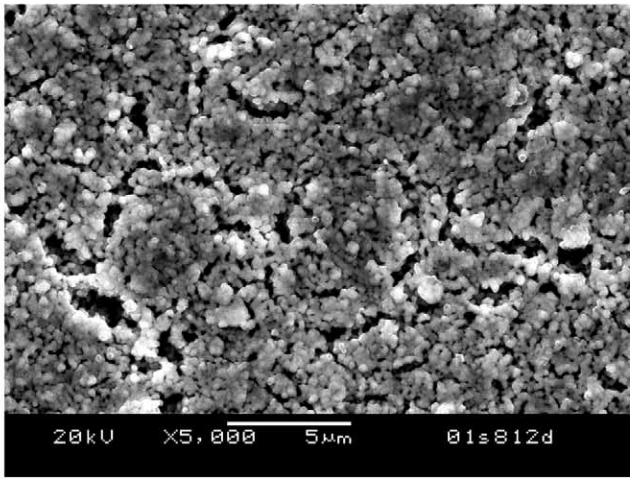

(b) – 2 mol% Co

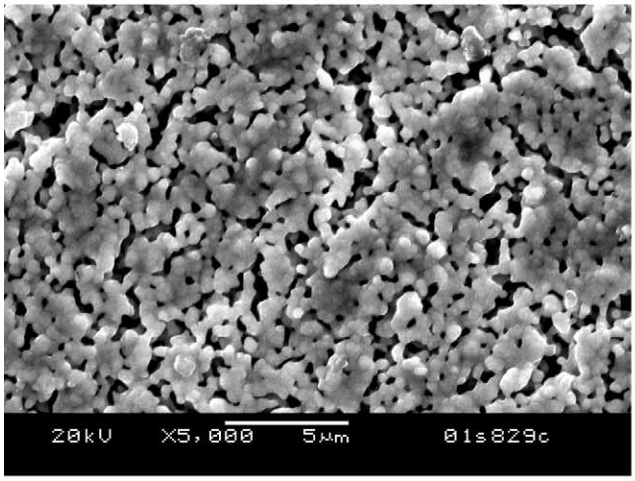

(c) – 2 mol% Cu

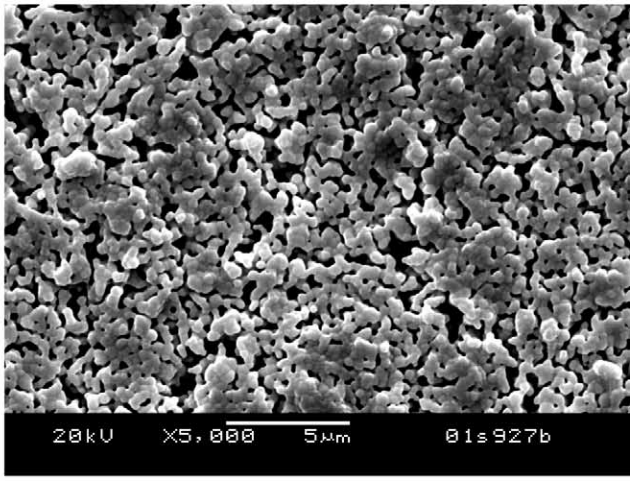

(d) – 2 mol% Fe

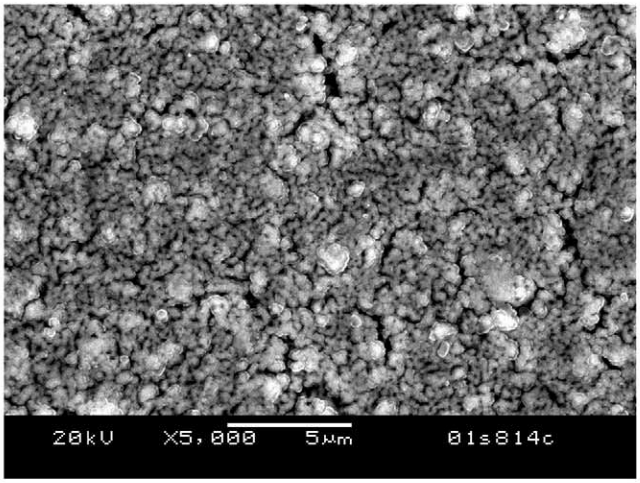

(e) – 2 mol% Ni

Fig. 11. SEM micrographs of screen-printed $Ce_{0.8}Sm_{0.18}M_{0.02}O_{1.9}$ films sintered onto the post-sintered anode–YSZ substrate—fired between 1000 and 1200 °C. (a) SDC-20; (b) 2 mol% Co; (c) 2 mol% Cu; (d) 2 mol% Fe; (e) 2 mol% Ni.

restricted to the "z" direction since the "x–y" plane remains constrained by the anode–YSZ support. There are of course many processing techniques that would yield a highly densified ceria layer such as PVD, ECVD, etc., though these methods are both slow and expensive, and a universal goal within the SOFC community is to develop an economical and commercially viable SOFC system. In an attempt to improve the sinterability of the SDC layer, 2 mol% of transition metal dopants were added to the SDC to give compositions $Ce_{0.8}Sm_{0.18}M_{0.02}O_{1.9}$ (where M = Co, Cu, Fe and Ni). Fig. 10 indicates the sintering shrinkage behavior of bulk samples of these materials. Similar findings were observed by Kleinlogel and Gauckler [15]. Each transition metal dopant addition produces enhanced sintering behavior with a lower sintering onset temperature than SDC-20 with no additional dopants. The subsequent expansion of the Cu- and Co-doped samples is the result of entrapped air where the surface of the sample has fully densified, so that any trapped air expands on further heating causing the sample to bloat. Figs. 11a–e show screen-printed layers of the aforementioned transition metal doped compositions, which were sintered from 1000 to 1200 °C. None of the compositions shows improved density compared to the base SDC material, and subsequent single cell testing with identical cathodes indicated the highest power densities for cells using the standard SDC material. Hence, although it's possible to improve the bulk sintering of SDC-20 with transition metal dopants, the "x–y" sintering restriction of the screen-printed layers still prevents complete densification of the ceria interlayer. Current studies are focused on improving the particle packing of the screen-printed layer to yield a higher green density and hence post-fired density.

3.3. LSF-20–SDC-20 cathode mixtures

Mixed LSM–YSZ compositions have received considerable attention, and show improved cell performance over pure LSM cathodes. As such, 20–60 wt.% SDC proportions were added to LSF-20 cathodes to evaluate the affects of incorporating a pure ionic conducting phase. The LSF–SDC layer was incorporated as a thin (5–10 μm) interfacial layer between the SDC and a bulk LSF cathode. Fig. 12 shows cell performances at 750 °C after 1 day of operation. The optimum power density is observed for an LSF-20–SDC-20 (60–40 wt.%) mixture (~650 mW/cm^2 at 750 °C/0.7 V), approximately 150–200 mW/cm^2 lower than pure LSF-20 cathodes. This should probably be expected since LSF-20 is a mixed conductor, and replacement of this phase with SDC may marginally enhance the ionic conductivity of the cathode, but is likely to significantly reduce the electronic conductivity.

3.4. Noble metal catalysts

A number of studies have been conducted on the catalytic benefits of small noble metal additions to SOFC cathodes

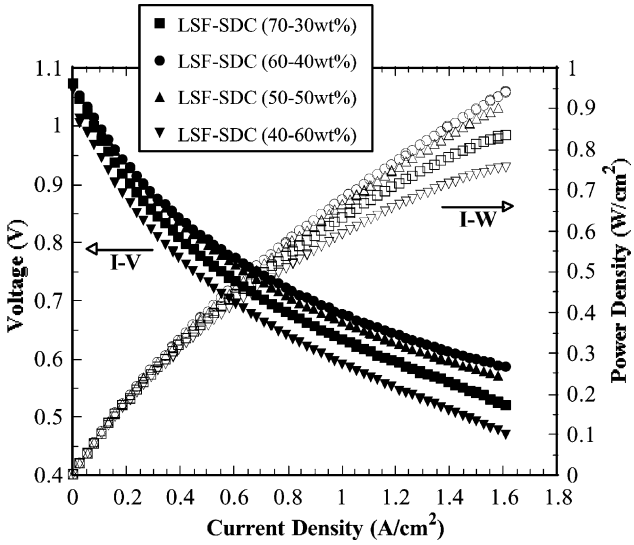

Fig. 12. Current and power density data for $La_{0.8}Sr_{0.2}FeO_{3-\delta}$–$Ce_{0.8}Sm_{0.2}O_{1.9}$ cathode mixtures.

[16–18]. For this study 1–2 vol.% Pd or Pt was added to either the base LSF-20 or to an LSF-20–SDC-20 (60–40 wt.%) cathode. Noble metals were incorporated into the cathodes via two methods: (1) diammine–palladium (or –platinum)II nitrite (Strem Chemicals) was added to the pre-combusted La–Sr–Fe nitrate solution; (2) high surface area Pd or Pt (~20 m^2/g, Alfa Aesar) was milled with post-synthesized LSF-20 powders. A thin (~5 μm post-sintered) layer of the Pd/Pt containing cathodes was screen-printed onto the sintered ceria interlayer followed by a bulk LSF-20 cathode (~40 μm post-sintered thickness). Fig. 13 shows an SEM micrograph of a Pd containing cathode. Fig. 14 indicates the performance of 2 vol.% additions of Pd or Pt to the LSF–SDC mix. Compared to the base LSF–SDC the Pd addition results in a 50% power density improvement at 0.7 V/700 °C, whereas the Pt addition affords no discernible enhancement. Similar trends were obtained for Pd/Pt additions to the LSF-20. However, long-term testing of samples incorporating Pd indicates performance instability. Fig. 15 shows a long-term plot (700 °C/0.7 V) for a cell utilizing an LSF-20 cathode with 2 vol.% Pd. After 2 h the performance reached a maximum of ~610 mW/cm^2 followed by a rapid degradation in less than 24 h to <400 mW/cm^2 (comparable to the power density of a cell without Pd additions). Thus, it appears that Pd facilitates initial cathode improvements with respect to the catalytic activity for O_2 reduction, but this enhancement is not sustainable. A tentative reason for the observed performance decrease may be related to the migration of Pt to the cathode–SDC interface during cell operation. This phenomenon was reported in a previous study conducted at PNNL [8], and is believed to be related to the volatilization of Pt-O species at the surface of the Pt current collector, and subsequent reduction to Pt metal at the cathode–SDC interface; the fact that no Pt is ever observed in the bulk cathode

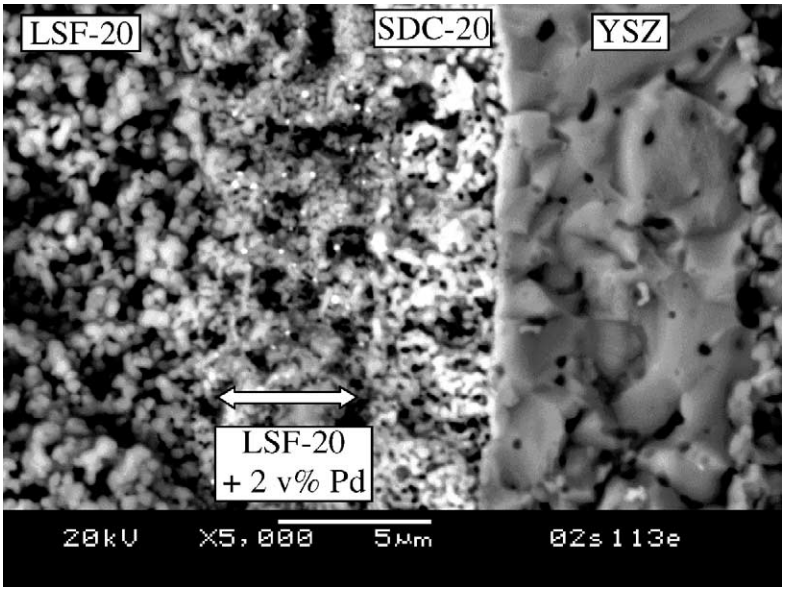

Fig. 13. SEM micrograph of a $La_{0.8}Sr_{0.2}FeO_{3-\delta}$ bulk cathode with a 5 μm $La_{0.8}Sr_{0.2}FeO_{3-\delta}$ + 2 vol.% Pd active cathode layer.

probably rules out solid state or surface diffusion processes. It should also be noted that this phenomenon only occurs when the cell is discharged electrically for a period of time (rather than being merely held at temperature). SEM/EDX examination of Pd containing cells show that after only 24 h of operation the Pd particles have become significantly alloyed with Pt, which has presumably migrated from the cathode current collector. From Fig. 14 it is evident that Pt does not aid the cathode reaction processes, and the alloying of Pt with the Pd particles may be responsible for the observed degradation phenomenon. Hence, at present it is uncertain if Pd will give long-term improvements in cell performance and the exact role (if any) of Pt the aforementioned instability must be assessed. To accurately establish this, the Pt current collector should be completely removed, and work is currently underway to design/fabricate an alternative cell fixture configuration that would not require a Pt cathode current collector.

3.5. High ionic conductors as interfacial cathode phases

It is generally accepted that improved ionic conductivity with the cathode close to the electrolyte interface should significantly improve the cathode activity. However, as reported by Ullmann et al. [19] there is a proportional linear relationship between ionic conductivity and thermal expansion coefficient (TEC). The anode support structure has a TEC close to $12 \times 10^{-6}\ ^{\circ}C^{-1}$, and hence the need to avoid large thermal mismatches limits the TEC of other cell components. However, it was considered that a very thin

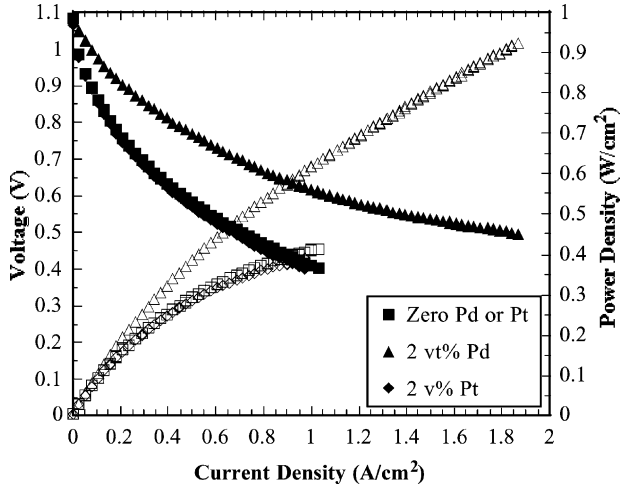

Fig. 14. Current and power density data for $La_{0.8}Sr_{0.2}FeO_{3-\delta}$ bulk cathodes with $La_{0.8}Sr_{0.2}FeO_{3-\delta}$–$Ce_{0.8}Sm_{0.2}O_{1.9}$ (60–40 wt.%) active cathode mixtures containing 2 vol.% Pd or Pt.

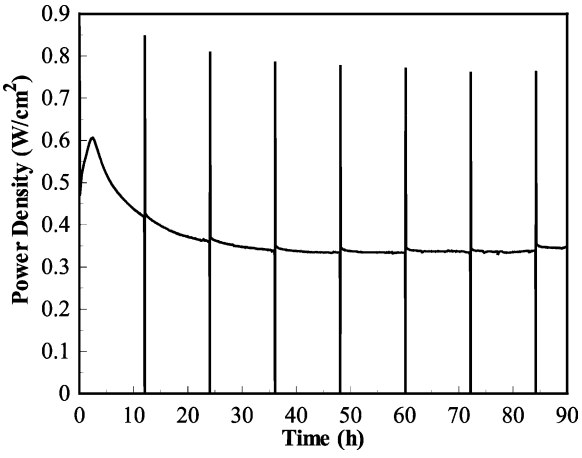

Fig. 15. Long-term performance data at 700 °C/0.7 V for a $La_{0.8}Sr_{0.2}FeO_{3-\delta}$ bulk cathode with $La_{0.8}Sr_{0.2}FeO_{3-\delta}$ active cathode mixture containing 2 vol.% Pd.

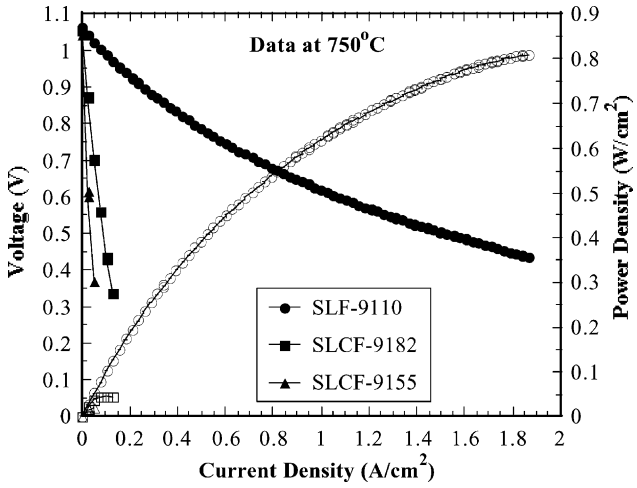

Fig. 16. Current and power density data for $La_{0.8}Sr_{0.2}FeO_{3-\delta}$ bulk cathodes with thin interfacial $Sr_{0.9}La_{0.1}Co_xFe_{1-x}O_{3-\delta}$ cathode layers ($x = 0$, 0.2 and 0.5 denoted by SLF-9110, SLCF-9128, and SLCF–9155, respectively).

high ionic conducting layer between the LSF-20 and SDC-20 layers may have less induced stress resulting from any thermal expansion mismatches. Compositions of the type $Sr_{0.9}La_{0.1}Co_xFe_{1-x}O_{3-\delta}$ ($x = 0$, 0.2 and 0.5 denoted by SLF-9110, SLCF-9128, and SLCF-9155, respectively) were considered. Fig. 16 indicates *IV–IW* data for cells incorporating the aforementioned layers at 750 °C. The Co-containing compounds have significantly reduced performance compared to the straight Sr-La-Fe-O compound (SLF-9110), but even this compound indicates considerably lower power densities compared to the base LSF-20 cathode (SLF-9110, ~525 mW/cm^2, LSF-20, ~800 mW/cm^2 at 750 °C/0.7 V). The phenomenon responsible for the poor performance of these cathode configurations is readily apparent from the SEM micrograph in Fig. 17, which shows a 1 μm thick interfacial phase, identified by EDX as Sr-Zr-O rich (probably a resistive Sr-zirconate phase), between the SDC interlayer and YSZ electrolyte. Presumably during sintering of the cathode a liquid phase was formed within the SLCF layer, which subsequently wicked through the porous SDC layer and reacted at the YSZ interface. All three compositions indicated the presence of the Sr-Zr-O layer, the thickness of which increased with Co content. Hence, though the SLCF layer appears well adhered without any discernible cracking resulting from potential thermal mismatch induced stresses the presence of the detrimental liquid phase is likely to inhibit the use of the aforementioned interfacial layers or the incorporation of the SLCF phases as a second phase mixed in with the LSF. However, if the resulting reaction layer arises from liquid wicking through the ceria, the ability to better densify the ceria layer may prevent the liquid diffusion to the SDC–YSZ interface and subsequent reaction.

3.6. Long-term cell stability

Whilst substantial cathode improvements are still necessary to facilitate increased power densities for low temperature SOFCs, an equally important goal is that of long-term stability. There are many phenomena that can affect long-term cell performance including chemical interaction of adjacent cell components to form insulating phases, volatilization of chemical species (e.g. Cr in the case of Cr containing alloy separator plates), and sintering of the cathode and/or anode. Despite the importance of long-term cell performance, little extended cell data has been presented in the published literature for the array of cathodes currently being studied in the SOFC community. With our own research instability has been observed for $La(Sr)CoO_3$

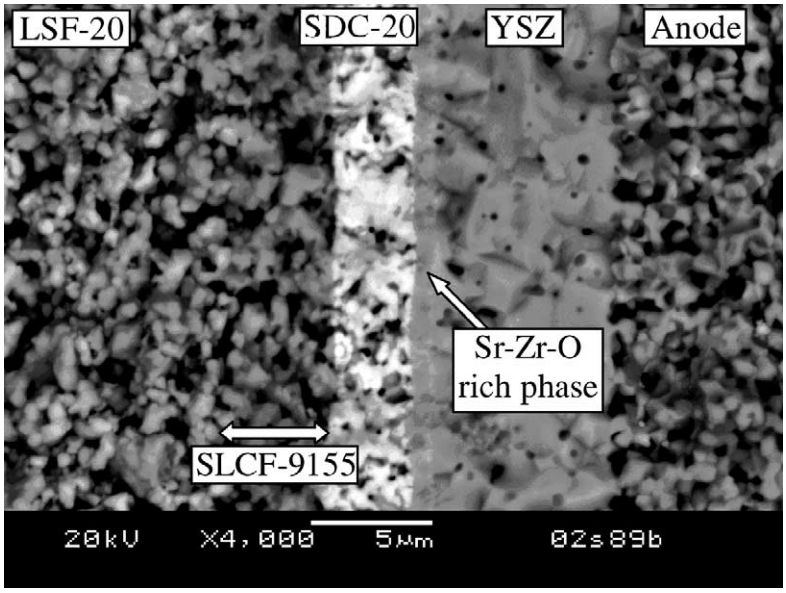

Fig. 17. SEM micrograph depicting Sr-Zr-O rich phase at the YSZ–SDC interface for a cell utilizing a $La_{0.8}Sr_{0.2}FeO_{3-\delta}$ bulk cathode with a thin interfacial $Sr_{0.9}La_{0.1}Co_{0.5}Fe_{0.5}O_{3-\delta}$ layer.

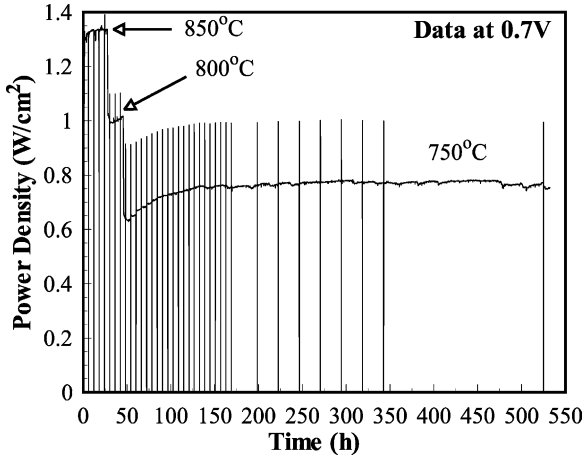

Fig. 18. Long-term performance data for an $La_{0.8}Sr_{0.2}FeO_{3-\delta}$ cathode at 750 °C and 0.7 V.

and La(Sr)Fe(Ni)O_3 cathodes—the former indicated phase separation and Co diffusion at 750 °C/0.7 V. However, LSF-20 has shown very promising long-term data. Fig. 18 illustrates the most recent long-term performance data of an anode-supported YSZ cell utilizing a base LSF-20 cathode. After initial data acquisition at 850 and 800 °C the cell was held at 0.7 V and 700 °C, and achieved a power density of 770 mW/cm^2 with no discernible degradation over a 500 h period. The vertical lines on the graph are the result of periodic *IV* sweeps.

4. Conclusions

Research with respect to improved activity SOFC cathodes is of paramount importance to realize the commercialization of low temperature (high performance) SOFCs. At PNNL reasonable success has been achieved towards this goal with the use of anode-supported SOFCs utilizing a thin YSZ electrolyte and Sr-doped lanthanum ferrite cathode. Current studies (not all detailed in this paper) involve optimizing the base LSF-20 cathode with respect to microstructure and thickness, the incorporation of high electronic conducting bulk cathodes, e.g. lanthanum nickel ferrites, with an LSF-20 active cathode layer to reduce sheet resistances and aid current collection, engineering the cathode–ceria interlayer interface to maximize the contact area (triple phase boundaries), maximizing the sintered density of the ceria layer (since it is essentially an extension of the electrolyte), understanding the role of the ceria interlayer to enable possible removal of said layer while maintaining high performance (previous tests have shown more than a doubling in power density for an YSZ–SDC–LSF configuration compared to YSZ–LSF), compositional modification of the base LSF-20 material to induce higher electronic/ionic conductivities, and the addition of noble metal phases to an active cathode layer to enhance the oxygen reduction reaction. As demonstrated by this article not all of these research avenues will necessarily lead to improved cathode performance, but it is envisaged that they will provide a better understanding of this particular cathode system, and a basis on which to eventually exact significant enhancements in low temperature power and cell longevity.

Acknowledgements

The authors would like to thank Jim Coleman for SEM/EDX analysis. The work summarized in this paper was funded as part of the Solid-State Energy Conversion Alliance (SECA) Core Technology Program by the US Department of Energy's National Energy Technology Laboratory (NETL). PNNL is operated by Battelle Memorial Institute for the US Department of Energy under Contract DE-AC06-76RLO 1830.

References

[1] S.P. Simner, J.F. Bonnett, N.L. Canfield, K.D. Meinhardt, V.L. Sprenkle, J.W. Stevenson, Electrochem. Solid State Lett. 5 (7) (2002) A173.
[2] L.A. Chick, L.R. Pederson, G.D. Maupin, J.L. Bates, L.E. Thomas, G.J. Exarhos, Mater. Lett. 10 (1–2) (1990) 6.
[3] S.P. Simner, J.S. Hardy, J.W. Stevenson, T.R. Armstrong, J. Mater. Sci. 34 (1999) 5721.
[4] S.P. Simner, J.S. Hardy, J.W. Stevenson, T.R. Armstrong, J. Mater. Sci. Lett. 19 (2000) 863.
[5] L.A. Chick, J. Liu, J.W. Stevenson, T.R. Armstrong, D.E. McCready, G.D. Maupin, G.W. Coffey, C.A. Coyle, J. Am. Ceram. Soc. 80 (8) (1997) 2109.
[6] K. Eguchi, N. Akasaka, H. Mitsuyasu, Y. Nonaka, Solid State Ionics 135 (2000) 589.
[7] K. Eguchi, T. Setoguchi, T. Inoue, H. Arai, Solid State Ionics 52 (2000) 165.
[8] S.P. Simner, J.W. Stevenson, K.D. Meinhardt, N.L. Canfield, Solid oxide fuel cells VII, in: H. Yokokawa, S.C. Singhal (Eds.), The Electrochemical Society Proceedings Series, Pennington, NJ, 2001, PV 2001-16, p. 1051.
[9] J.M. Ralph, J.T. Vaughey, M. Krumpelt, Solid oxide fuel cells, vol. VII, in: H. Yokokawa, S.C. Singhal (Eds.), The Electrochemical Society Proceedings Series, Pennington, NJ, 2001, PV 2001-16, p. 466.
[10] M. Mori, T. Abe, H. Itoh, O. Yamamoto, G.Q. Shen, Y. Takeda, N. Imanishi, Solid State Ionics 123 (1999) 113.
[11] H.Y. Lee, S.M. Oh, Solid State Ionics 90 (1996) 133.
[12] A. Mitterdorf, L.J. Gauckler, Solid State Ionics 111 (1998) 185.
[13] G.C. Kostogloudis, G. Tsiniarakis, C. Ftikos, Solid State Ionics 135 (2000) 529.
[14] F.M. Figueiredo, J.A. Labrincha, F.M.B. Marques, Solid State Ionics 101–103 (1997) 343.
[15] C. Kleinlogel, L.J. Gauckler, Solid Oxide Fuel Cells VI, in: H. Yokokawa, S.C. Singhal (Eds.), The Electrochemical Society Proceedings Series, Pennington, NJ, 1999, PV 99-19, p. 225.
[16] J.W. Erning, T. Hauber, U. Stimming, K. Wippermann, J. Power Sources 61 (1996) 205.
[17] H. Uchida, S. Arisaka, M. Watanabe, Solid State Ionics 135 (1–4) (2000) 347.
[18] M. Sahibzada, S.J. Benson, R.A. Rudkin, J.A. Kilner, Solid State Ionics 113–115 (1998) 285.
[19] H. Ullmann, N. Trofimenko, F. Tietz, D. Stöver, A. Ahmad-Khanlou, Solid State Ionics 138 (1–2) (2000) 79.